BMC Neurology

RESEARCH

Open Access

Feasibility of a clinical-radiomics combined model to predict the occurrence of stroke-associated pneumonia

Haowen Luo[1†], Jingyi Li[1,2†], Yongsen Chen[1,2], Bin Wu[1,2], Jianmo Liu[1], Mengqi Han[1,2], Yifan Wu[1,2], Weijie Jia[1,2], Pengfei Yu[1], Rui Cheng[1,2], Xiaoman Wang[1,2], Jingyao Ke[1,2], Hongfei Xian[1,2], Jianglong Tu[3*] and Yingping Yi[1*]

Abstract

Purpose To explore the predictive value of radiomics in predicting stroke-associated pneumonia (SAP) in acute ischemic stroke (AIS) patients and construct a prediction model based on clinical features and DWI-MRI radiomics features.

Methods Univariate and multivariate logistic regression analyses were used to identify the independent clinical predictors for SAP. Pearson correlation analysis and the least absolute shrinkage and selection operator with ten-fold cross-validation were used to calculate the radiomics score for each feature and identify the predictive radiomics features for SAP. Multivariate logistic regression was used to combine the predictive radiomics features with the independent clinical predictors. The prediction performance of the SAP models was evaluated using receiver operating characteristics (ROC), calibration curves, decision curve analysis, and subgroup analyses.

Results Triglycerides, the neutrophil-to-lymphocyte ratio, dysphagia, the National Institutes of Health Stroke Scale (NIHSS) score, and internal carotid artery stenosis were identified as clinically independent risk factors for SAP. The radiomics scores in patients with SAP were generally higher than in patients without SAP ($P < 0.05$). There was a linear positive correlation between radiomics scores and NIHSS scores, as well as between radiomics scores and infarct volume. Infarct volume showed moderate performance in predicting the occurrence of SAP, with an AUC of 0.635. When compared with the other models, the combined prediction model achieved the best area under the ROC (AUC) in both training (AUC = 0.859, 95% CI 0.759–0.936) and validation (AUC = 0.830, 95% CI 0.758–0.896) cohorts ($P < 0.05$). The calibration curves and decision curve analysis further confirmed the clinical value of the nomogram. Subgroup analysis showed that this nomogram had potential generalization ability.

Conclusion The addition of the radiomics features to the clinical model improved the prediction of SAP in AIS patients, which verified its feasibility.

Keywords Stroke-associated pneumonia, Radiomics, Prediction, Acute ischemic stroke, Magnetic resonance imaging

†Haowen Luo and Jingyi Li contributed equally to this work and share first authorship.

*Correspondence:
Jianglong Tu
Tujianglong85@126.com
Yingping Yi
yyp66@126.com
Full list of author information is available at the end of the article

Introduction

Stroke-associated pneumonia (SAP) is one of the most common medical complications in patients with acute ischemic stroke (AIS), with an estimated incidence ranging between 5 and 26% [1]. SAP reduces the quality of life and increases the treatment costs, hospital stay, and risk of mortality in AIS patients [2–6]. Therefore, there is a need to develop fast and reliable tools to identify high-risk patients to improve clinical outcomes.

Previous studies have established different scoring systems for early pneumonia prediction after AIS, such as the A2DS2 scale, the AIS-APS scale, and the ISAN scale [7–9]. However, these tools are based solely on clinical data, and their prediction efficiency is moderate [10]. Brain imaging is necessary to diagnose stroke and evaluate the extent of the disease. Diffusion-weighted imaging-magnetic resonance imaging (DWI-MRI) is the most sensitive and accurate imaging method for diagnosing AIS and has been widely used in studies related to stroke [11, 12]. Several studies identified a correlation between the brain infarct size on DWI-MRI and prognosis following an AIS and may also have a role in the development of complications [13–15]. Studies have also found an association between several MRI radiological features, including the location, infarct volume, the number of lobes involved, and the brain atrophy score, with the risk of developing SAP [16, 17].

Radiomics uses algorithms to objectively extract a large number of quantitative features from medical images. This data can be used to transform subjective visual evaluation into an objective evaluation data-driven evaluation of traditional radiologic characteristics [18–22]. This technique is increasingly being used to facilitate the diagnosis of stroke lesions [23, 24], predict early outcomes [25–27], and evaluate the long-term prognosis of stroke [28, 29]. However, to our knowledge, no studies have been conducted evaluating the role of radiomics in predicting SAP following an AIS.

Therefore, in this study, we aimed to explore the predictive value of radiomics in predicting SAP and construct a prediction model based on clinical features and DWI-MRI radiomics features to predict SAP following AIS. The model was developed into a nomogram, and decision curve analysis (DCA) was performed to evaluate the clinical utility of the model.

Materials and methods

Study population

AIS patients who underwent a DWI-MRI scan from January 2018 to December 2021 were selected from our institution. All patients aged 18 years or above who were immediately hospitalized within 24 h following the onset of AIS symptoms and had a confirmed diagnosis of AIS on DW-MRI as defined by the World Health Organization [30, 31] and a National Institute of Health stroke scale (NIHSS) score of 15 or less were included in the study. Patients that presented with diseases that had clinical symptoms similar to pneumonia, such as pulmonary edema, pulmonary embolism, pulmonary atelectasis, tuberculosis, pulmonary tumor, and non-infective interstitial lung disease ($n=3$), and those who had pneumonia before admission ($n=17$) were excluded from the study. In addition, patients who lacked the complete clinical data ($n=276$) and those who lacked an MRI or had severe artifacts on MRI ($n=16$) were also excluded. The patients' enrollment flow chart was illustrated in Fig. 1. Finally, 298 patients were included. None of the patients underwent intravenous thrombolysis. The patients were randomly divided into a training cohort ($n=208$) and a validation cohort ($n=90$) at a ratio of 7:3.

Diagnostic criteria for SAP

SAP was defined as a 'spectrum of lower respiratory tract infections occurring within the first 7 days after the onset of stroke'. Clinicians diagnosed SAP according to the data retrieved from chest images, clinical signs and symptoms, and laboratory parameters per guidelines issued by the Centers for Disease Control and Prevention criteria (CDC) [32]. The patients diagnosed with SAP were recorded and were divided into the SAP and non-SAP groups according to the criteria above.

Ethical considerations

The study was approved by the Medical Ethics Committee of our institution: (2018) Medical Research Review No.04. Written informed consent was obtained from all patients participating in this study.

Clinical data extraction

The clinical data, including demographics, past history, comorbidities, characteristics of condition on admission, laboratory results and image features, were extracted for the first time after admission and retrieved from the patient's medical records. The demographics included age, sex and body mass index (BMI). Past history included smoking and stroke. Comorbidities included hypertension, diabetes and dyslipidemia. Characteristics of condition on admission included dysphagia, NIHSS score, and the Modified Rankin Scale (mRS) score. The mRS score was used to measure the level of disability following AIS. Based on this score, the patients were divided into functionally independent if they had an mRS score of 2 or less and functionally dependent if they had an mRS score above 2 [33, 34]. Laboratory results included platelets (PLT), creatinine (Cr), aspartate transaminase to alanine transaminase ratio (AST/ALT), total cholesterol

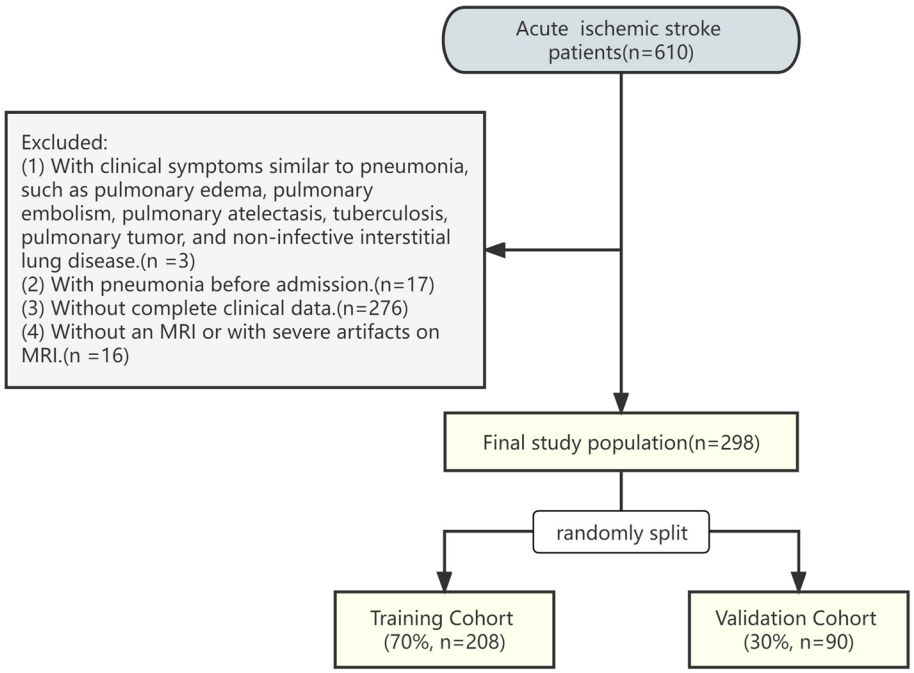

Fig. 1 The flow chart of patients' enrollment

(Tch), low-density lipoprotein (LDL), high-density lipoprotein (HDL), triglycerides (TG), fasting plasma glucose (FPG), homocysteine (HCY), albumin (ALB), and the neutrophil to lymphocyte ratio (NLR). Image features included stenosis location (internal carotid artery (ICA), middle cerebral artery (MCA)), the extent of the stenosis (more or less than 50%), infarction side (left, right, or bilateral) and volume.

MRI acquisition

All patients underwent a DWI-MRI within 24 h of admission. The DWI-MRIs were acquired using a GE 3.0 T MRI scanner, using a repetition time (TR) of 4090 ms, an echo time (TE) of 98.0 ms, a field of view (FOV) = 230 mm x 230 mm, a matrix of 192 × 192, a slice thickness to gap ration of 5 mm/1.5 mm, a b value of 0, and 1000 s/mm^2.

Lesion site annotating and feature extraction

The radiomics analysis process was divided into 4 phases; lesion site annotation, feature extraction, feature selection, and model construction (Fig. 2). Two radiologists annotated the ischemic lesions on the patient's DWI using the 3D-Slicer software version 4.10.2. Then, the consistency of the annotated volumes was evaluated by calculating the intra-class correlation coefficients (ICC). An ICC greater than 0.75 indicates a good agreement [35].

Subsequently, radiomics features were extracted using the PyRadiomics version 3.0.1 software as indicated by the Image Biomarker Standardization Initiative [36]. These features included first-order, shape and texture. The first-order and texture features were extracted from the original image, the Gaussian Laplace filtered image, and the wavelet filtered image.

Feature selection and model construction

Univariate analysis was used to identify the factors that differed between all patients that developed SAP and those that did not. Then, the significant variables in the training cohort were inputted into the multivariate logistics regression (MLR) model to determine the independent clinical predictors of SAP ($P < 0.05$). These features were then used to construct the clinical prediction model. The risk ratios of the predicted factor were expressed as odds ratio (OR) (95% confidence interval).

Spearman's correlation coefficient was used to calculate the correlation and redundancy of features in the training cohort. The features were classified as redundant if they had a Spearman correlation coefficient higher than 0.8. For each pair of features that have been marked as redundant, choose to retain one of the features, the other redundant feature was removed [37]. Subsequently, the optimal predictive features were screened out utilizing the least absolute shrinkage and selection operator (LASSO) with ten-fold cross-validation [38]. Eventually, the radiomics score was calculated for each patient based on the linear combination of weighted selection parameters for the relevant LASSO coefficients of the optimal

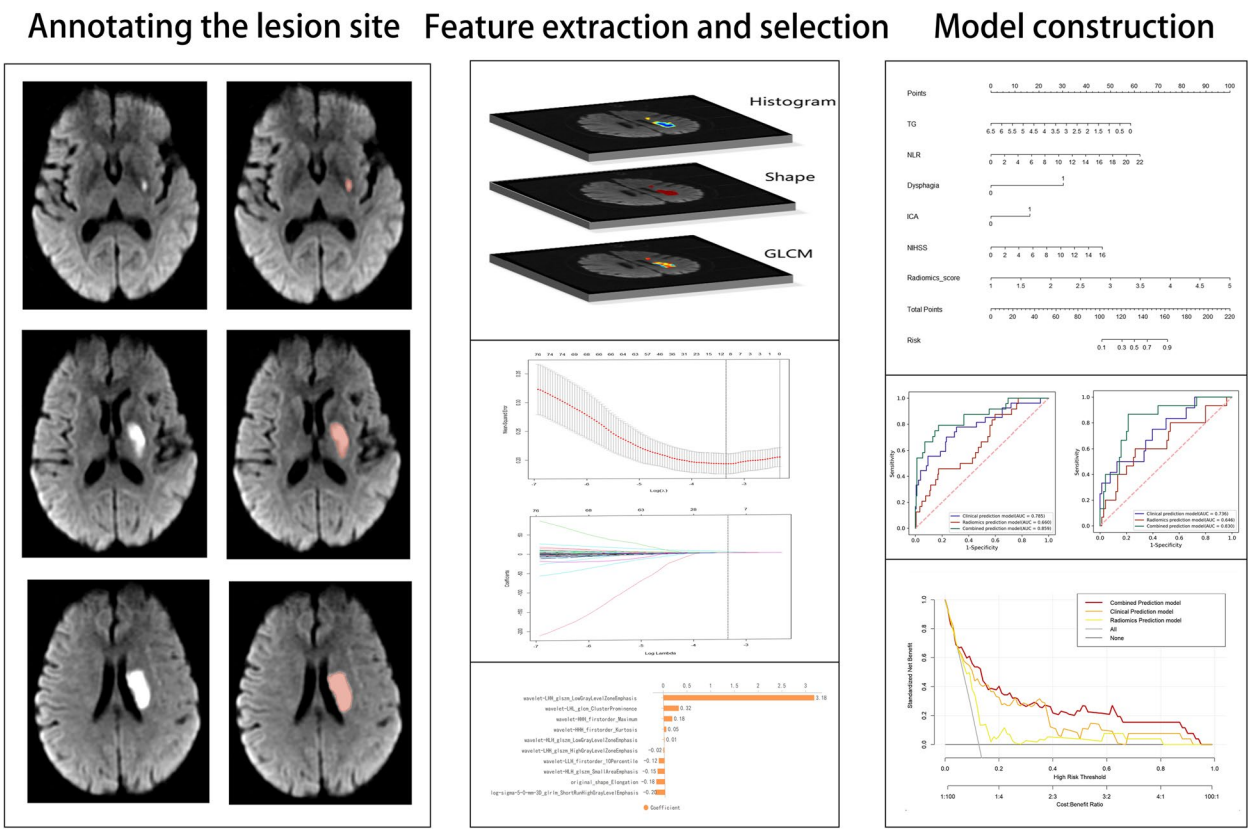

Fig. 2 Flowchart of radiomics analysis

features, which was used to construct the radiomics prediction model. Finally, a combined prediction model was built based on both radiomics and clinical features, as well as a clinical prediction model containing only the clinical features and a radiomics prediction model containing only the radiomics features were built for comparison. Then, the best-performing model was developed into a nomogram. Subsequently, a subgroup analysis was performed based on age, sex, BMI, and stroke severity on admission to test the generalization ability of our model.

Statistical analyses

The Python software (version 3.0) and R software (version 4.2.1) were used for statistical analyses. The normally distributed variables were expressed as mean ± standard deviation (SD), while the non-normally distributed variables were expressed as median (first quartile, third quartile). The variables between the SAP and non-SAP groups were compared using the student's t-test for the normally distributed variables and the Mann–Whitney U test for the non-normally distributed variables. The categorical variables were expressed as numbers (percentage), and the chi-squared ($\chi 2$) test was used for comparison. Pearson correlation analysis was used to test the correlation. The predictive performance of all 3 models was compared by calculating the area under the curve (AUC) of a receiver operating characteristics curve (ROC), the accuracy, sensitivity, specificity, negative predictive values (NPV), and positive predictive values (PPV). The Delong test was used to compare the differences in ROC curves between the models. The nomogram's accuracy was evaluated using calibration curves [39]. A decision curve analysis (DCA) was used to evaluate the clinical value of the nomogram in the validation cohort [40]. For all statistical tests, a p-value below 0.05 was considered statistically significant.

Results

Clinicodemographic features

The clinicodemographic features of the SAP and non-SAP patients in the training and validation cohorts are summarized in Table 1. A total of 298 patients were enrolled in this study, of whom 208 were assigned to the training cohort, and 90 were assigned to the validation cohort randomly. Of the 298 patients enrolled in the study, 39 (13.09%) patients developed SAP within 7 days following admission. A significant difference was noted in the age, BMI, dysphagia, NIHSS score, mRS score (> 2), TG, NLR,

Table 1 Risk factors in the training and validation cohorts

Characteristics	Training Cohort ($n=208$)			Validation Cohort ($n=90$)		
	Without SAP ($n=180$)	With SAP ($n=28$)	*P*	Without SAP ($n=79$)	With SAP ($n=11$)	*P*
Demographics						
Age, M(Q25,Q75)	63.00(55.00,71.00)	68.50(60.00,76.00)	0.044	63.00(56.00,71.00)	66.00(61.00,77.00)	0.230
Sex, n(%)			0.250			0.957
Male	118(65.56)	22(78.57)		54(68.35)	8(72.73)	
Female	62(34.44)	6(21.43)		25(31.65)	3(27.27)	
BMI, M(Q25,Q75)	23.86(21.51,25.39)	21.34(20.20,24.61)	0.012	23.63(21.26,25.39)	22.46(20.76,23.66)	0.089
Past History						
Stroke, n(%)	54(30.0)	6(21.43)	0.480	22(27.85)	2(18.18)	0.752
Smoking, n(%)	62(34.44)	15(53.57)	0.082	24(30.38)	5(45.45)	0.510
Comorbidities						
Hypertension, n(%)	137(76.11)	19(67.86)	0.482	64(81.01)	8(72.73)	0.809
Diabetes, n(%)	68(37.78)	8(28.57)	0.465	34(43.04)	3(27.27)	0.504
Dyslipidemia, n(%)	43(23.89)	3(10.71)	0.188	16(20.25)	1(9.09)	0.635
Characteristics of condition on admission						
Dysphagia, n(%)	7(3.89)	8(28.57)	< 0.001	3(3.8)	4(36.36)	0.001
NIHSS score, M(Q25,Q75)	3.00(1.00,6.00)	4.00(2.00,10.00)	0.038	2.00(0.00,5.00)	5.00(2.00,12.00)	0.041
mRS score(> 2), n(%)	36(20.0)	13(46.43)	0.005	13(16.46)	4(36.36)	0.242
Laboratory results						
PLT, M(Q25,Q75)	206.50(174.00,240.00)	214.50(163.00,259.00)	0.829	199.00(164.00,227.00)	219.00(201.00,265.00)	0.061
Cr, M(Q25,Q75)	73.57(62.34,90.84)	72.35(65.55,82.69)	0.428	76.03(66.57,93.53)	78.33(59.64,85.72)	0.622
AST/ALT, M(Q25,Q75)	1.19(0.96,1.52)	1.36(1.09,1.55)	0.133	1.17(0.99,1.49)	1.31(0.95,1.44)	0.409
Tch, M(Q25,Q75)	4.67(4.04,5.20)	4.68(3.67,5.36)	0.518	4.67(4.16,5.19)	4.71(4.06,5.11)	0.735
LDL, M(Q25,Q75)	2.77(2.36,3.18)	2.73(2.02,3.39)	0.757	2.84(2.36,3.32)	2.92(2.42,3.39)	0.878
HDL, M(Q25,Q75)	1.07(0.93,1.31)	0.98(0.85,1.32)	0.360	1.02(0.92,1.29)	0.99(0.81,1.49)	0.907
TG, M(Q25,Q75)	1.43(1.11,2.03)	1.11(0.96,1.65)	0.019	1.59(1.17,2.02)	1.09(0.83,1.69)	0.036
FPG, M(Q25,Q75)	5.38(4.70,7.20)	5.42(4.42,5.79)	0.359	5.90(5.13,7.61)	5.44(5.11,6.16)	0.334
HCY, M(Q25,Q75)	14.16(11.54,18.14)	15.84(11.45,19.34)	0.361	14.54(11.68,18.12)	15.35(10.85,19.15)	0.956
ALB, M(Q25,Q75)	37.88(35.73,40.12)	37.02(33.86,38.22)	0.075	37.95(36.08,40.38)	36.35(35.07,38.16)	0.040
NLR, M(Q25,Q75)	2.65(1.91,3.62)	3.44(2.16,5.42)	0.008	2.61(2.05,3.70)	4.71(3.82,6.77)	< 0.001
Imaging features						
Stenosis location, n(%)						
ICA	19(10.56)	9(32.14)	0.007	8(10.13)	4(36.36)	0.054
MCA	42(23.33)	10(35.71)	0.241	21(26.58)	4(36.36)	0.749
Infarction side, n(%)						
Left	69(38.33)	7(25.00)	0.249	35(43.75)	3(27.27)	0.456
Right	75(41.67)	14(50.00)	0.533	29(36.25)	4(36.36)	0.755
Bilateral	31(17.22)	8(28.57)	0.242	20(25.32)	3(27.27)	0.818
Volume, M(Q25,Q75)	1.27(0.49,4.82)	4.08(0.85,16.07)	0.017	1.22(0.42,6.07)	1.84(0.40,16.18)	0.566

stenosis location (ICA) and volume between the SAP and non-SAP patients of the training cohort (all $P<0.05$).

Identification of the independent clinical predictors

The MLR identified TG, NLR, NIHSS score, dysphagia, and stenosis location (ICA) as independent predictors for SAP (Table 2). Based on the result of the MLR, the clinical prediction model was defined by the formula: Y = -1.059TG + 0.373NLR + 0.188NIHSS score + 2.433Dysphagia + 1.542stenosis location (ICA).

The association between stenosis location (ICA), infarct volume and SAP

The infarct volume was found to be significantly larger in patients with ICA stenosis than in patients without ICA stenosis ($P=0.006$) (Fig. 3A).

Table 2 Univariate and multivariable regression findings

Risk factor	β	SE	Wald	OR (95% CI)	*P*
TG	-1.059	0.485	4.77	0.347(0.134,0.897)	0.029
NLR	0.373	0.112	11.163	1.452(1.167,1.807)	0.001
NIHSS score	0.188	0.073	6.694	1.207(1.047,1.392)	0.01
Dysphagia	2.433	0.747	10.598	11.392(2.633,49.311)	0.001
Stenosis location (ICA)	1.542	0.633	5.939	4.674(1.352,16.155)	0.015

The infarct volume was found to be significantly larger in patients with SAP than in patients without SAP ($P=0.017$) (Table 1, Fig. 3B). In addition, both in patients with SAP and in patients without SAP, infarct volume was larger in patients with ICA stenosis.

Infarct volume showed moderate performance in predicting whether AIS patients would develop SAP, with an AUC of 0.635 (Fig. 4).

Feature extraction and radiomics scores

A total of 1041 features predictive of SAP were extracted. The 10 most relevant radiomics features for SAP in the training cohort were obtained by LASSO with ten-fold cross-validation (Fig. 5A-C). The distribution of

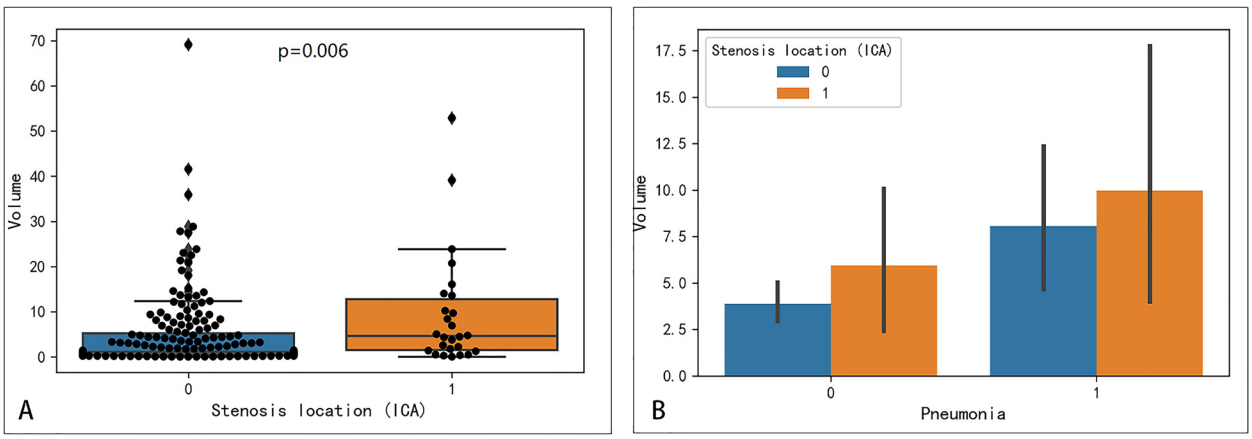

Fig. 3 The association between stenosis location (ICA), infarct volume and SAP. **A** The distribution of infarct volume in patients with ICA stenosis and patients without ICA stenosis. **B** The distribution of infarct volume in patients with SAP and patients without SAP

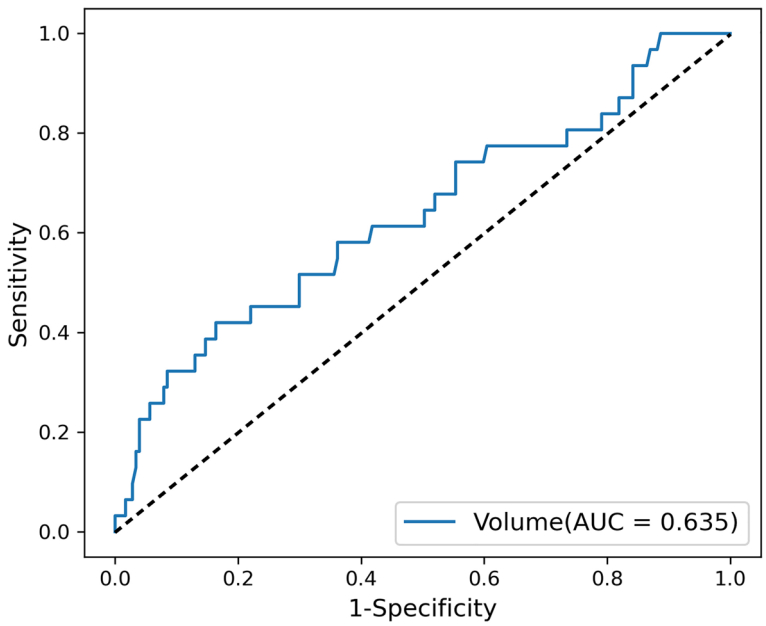

Fig. 4 Performance of infarct volume in predicting SAP

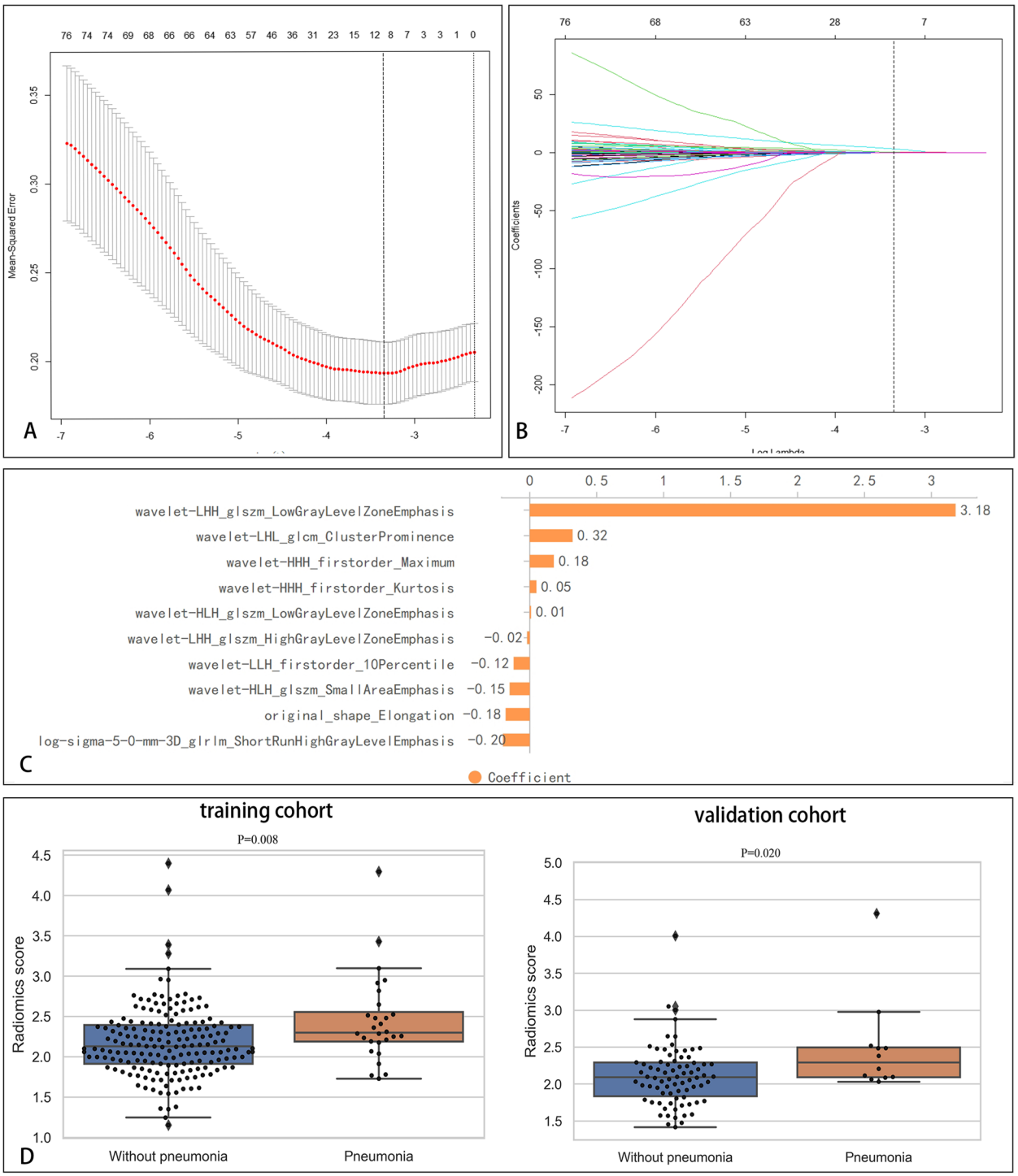

Fig. 5 The optimal radiomics features for SAP. **A** The tuning parameter (k) in the tenfold cross-validation LASSO model. **B** The coefficients plotted against log(k). **C** The most relevant radiomics features predictive of SAP. **D** The distribution of radiomics scores in the training and validation cohorts

the radiomics scores of patients with and without SAP for the training and validation cohorts is illustrated in Fig. 5D. The radiomics scores of patients with SAP and those without SAP were 2.30 (2.18, 2.65) and 2.13 (1.91, 2.40), respectively, for the training cohort and 2.29 (2.09, 2.52) and 2.09 (1.82, 2.29), respectively for the validation cohorts. The radiomics scores in patients with SAP were generally higher than in those without SAP. Wilcoxon's

test showed a significant difference in the radiomics scores between the patients with SAP in both the training and validation cohorts ($P < 0.05$). The mean ICC between the lesion volumes annotated by the 2 radiologists was 0.99 (95% CI 0.99–1, $P < 0.05$), indicating that the reproducibility of the feature extraction was good.

We investigated the association between radiomics scores and infarct volume as well as radiomics scores and independent risk factors (NIHSS, NLR, TG) (Fig. 6). The radiomics scores and NIHSS scores exhibited a positive linear relationship, with a Pearson correlation coefficient (r) of 0.171($P=0.014$) (Fig. 7A). The radiomics scores and volume exhibited a positive linear relationship, with a Pearson correlation coefficient (r) of 0.372($P < 0.001$) (Fig. 7B).

Prediction performance of the models

The prediction performance of the 3 models is summarized in Table 3, while Fig. 8 illustrates the ROCs for the 3 models. The clinical prediction model achieved an AUC of 0.785 (95%CI 0.673–0.889) and 0.736 (95%CI 0.629–0.837) for the training and validation cohorts, respectively. The sensitivity and specificity of the model were 0.667 and 0.768, respectively, in the training cohort and 0.417 and 0.872, respectively, in the validation cohort.

The radiomics prediction model achieved an AUC of 0.660 (95% CI 0.546–0.766) and 0.646 (95% CI 0.541–0.756) in the training and validation cohorts, respectively. The sensitivity and specificity of the model were 0.417 and 0.826, respectively, in the training cohort and 0.533 and 0.733, respectively, in the validation cohort.

The combined prediction model had an AUC of 0.859 (95% CI 0.759–0.936) and 0.830 (95% CI 0.758–0.896) in the training and validation cohorts, respectively. The sensitivity and specificity of the model were 0.750 and 0.826, respectively, in the training cohort and 0.800 and 0.787, respectively, in the validation cohort.

Compared with the other 2 models, the combined model had a significantly higher AUC in both the training

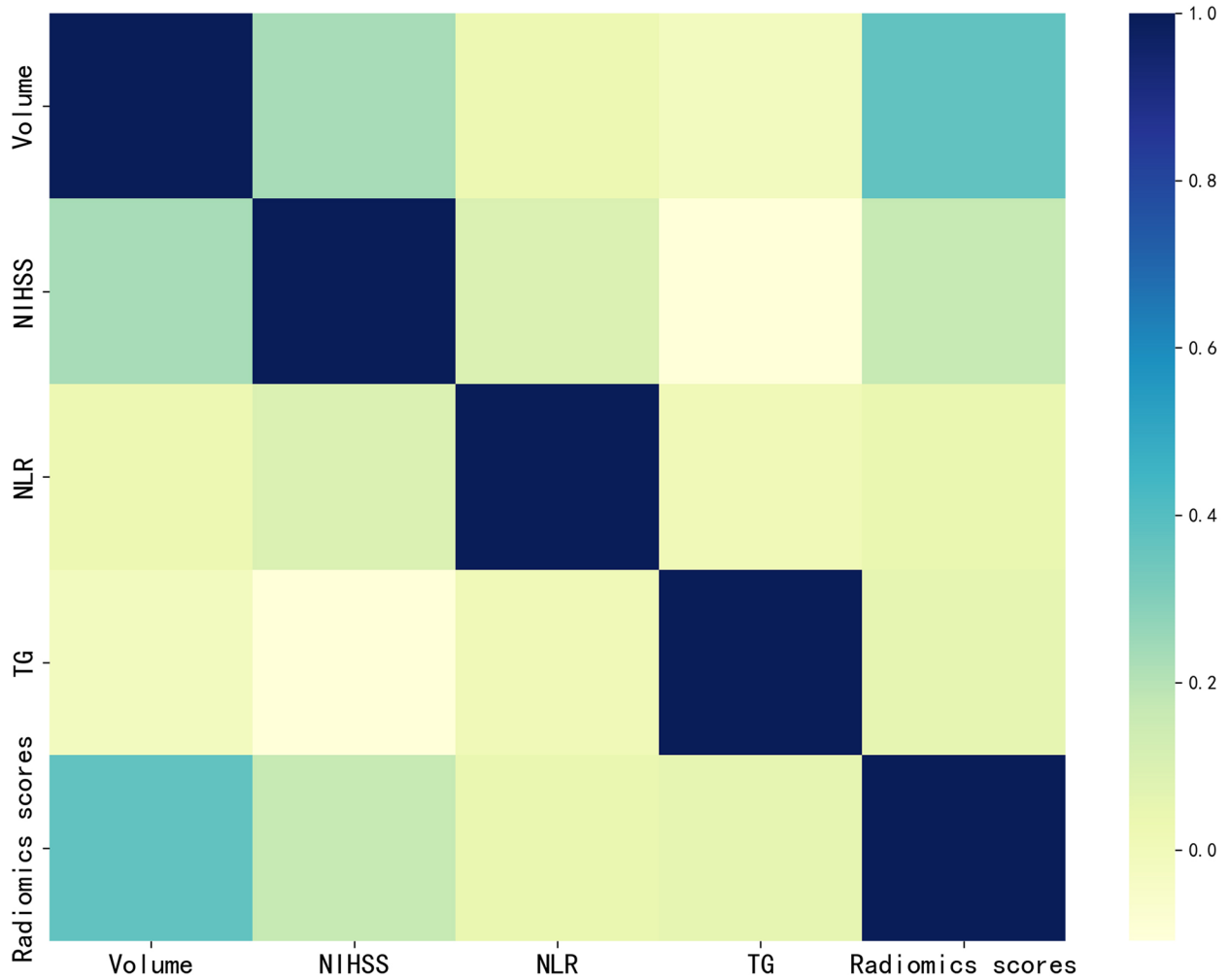

Fig. 6 Correlation analysis chart

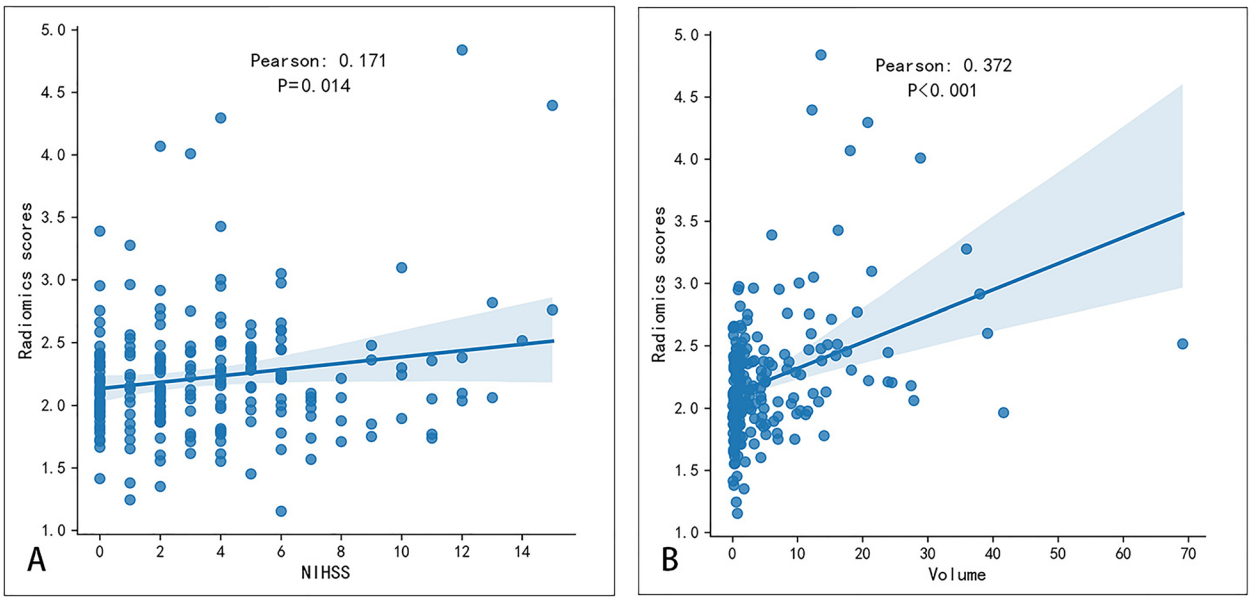

Fig. 7 The association between stenosis location (ICA), infarct volume and SAP. **A** Association between radiomics scores and NIHSS scores. **B** Association between radiomics scores and volume

Table 3 The performance of three prediction models in the training and validation cohorts

Model	Cohort	AUC (95%CI)	ACC	Sensitivity	Specificity	NPV	PPV
Radiomics Prediction model	Training Cohort	0.660(0.546–0.766)	0.779	0.417	0.826	0.916	0.238
	Validation Cohort	0.646(0.541–0.756)	0.700	0.533	0.733	0.887	0.286
Clinical Prediction model	Training Cohort	0.785(0.673–0.889)	0.759	0.667	0.768	0.939	0.300
	Validation Cohort	0.736(0.629–0.837)	0.811	0.417	0.872	0.907	0.333
Combined Prediction model	Training Cohort	0.859(0.759–0.936)	0.817	0.750	0.826	0.962	0.360
	Validation Cohort	0.830(0.758–0.896)	0.789	0.800	0.787	0.952	0.429

and validation cohorts (Delong test $P < 0.05$) (Table 4) and was therefore used to develop the clinical nomogram.

Development and validation of the nomogram

The nomogram of the combined model is illustrated in Fig. 9A. Clinicians could use the nomogram to predict the risk of developing SAP by summing the risk of the relevant clinical variables and the radiomics risk score. The calibration curves for the training and validation nomograms are illustrated in Fig. 9B. The calibration plot displayed a good level of consistency between the predicted and actual probabilities for both cohorts. The nomogram's DCA is displayed in Fig. 9C. The DCA confirmed the clinical utility of the model.

As shown in Table 5 and Fig. 10, the subgroup analysis showed that the performance of the nomogram was not influenced by patient age, sex, BMI and stroke severity on admission (Delong test $P > 0.05$).

Discussion

SAP is a potentially preventable complication of stroke. The early identification of SAP is essential to limit the adverse clinical outcome of pneumonia [41, 42]. In this study, we explored the predictive value of radiomics in predicting SAP and construct an artificial intelligent model based on clinical features and DWI-MRI radiomics features to predict SAP following AIS. The combined model performed better than clinical model and radiomics model. The DCA confirmed the clinical effectiveness of the proposed model.

It has been confirmed by several studies that brain MRI-based imaging features are closely related to SAP. Zhao et al. [43] showed that the DWI Alberta Stroke Program Early Computed Tomography Score (DWI-ASPECTS) used to predict the severity of AIS could also be used to predict the occurrence of SAP in patients with mild AIS [1, 44]. We investigated the association between radiomics scores, infarct volumes and NIHSS scores, found that

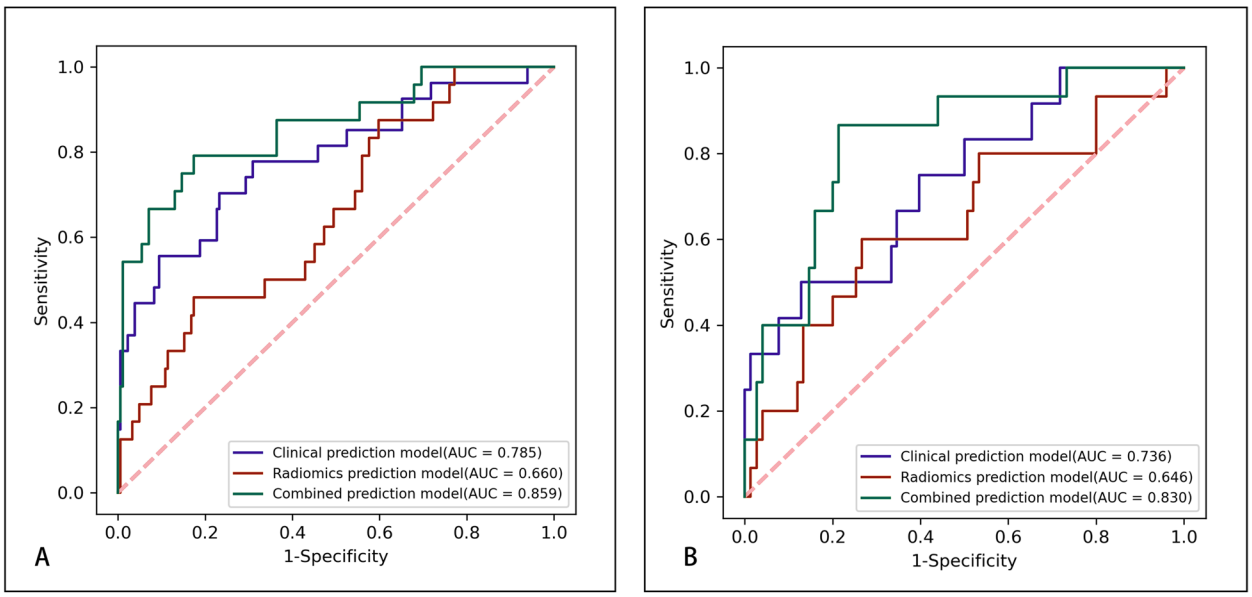

Fig. 8 ROC curves of the 3 prediction SAP models for the training (**A**) and validation (**B**) cohorts

Table 4 Comparison of ROC between the models using the Delong test

Cohort	The models for comparison	*P*
Training Cohort	Combined Prediction model versus Clinical Prediction model	0.042
	Combined Prediction model versus Radiomics Prediction model	0.006
Validation Cohort	Combined Prediction model versus Clinical Prediction model	0.043
	Combined Prediction model versus Radiomics Prediction model	0.05

there was a linear positive correlation between radiomics scores and NIHSS scores (Pearson:0.171, $P=0.014$), as well as between radiomics scores and infarct volume (Pearson:0.372, $P<0.001$). Yu et al. [17] found that neuroimaging features play a key role in predicting SAP. Brain atrophy and core infarct volume are closely related to the occurrence of SAP [45, 46]. We found that larger infarct volume and higher radiomics score were associated with a greater risk of developing pneumonia. We also investigated the predictive performance of infarct volume and obtained moderate performance, with an AUC of 0.635. The NIHSS score reflects the severity of the stroke [47]. Previous studies have shown that stroke severity increases the risk of developing SAP [1]. Therefore, the radiomics score reflects the severity of stroke to a certain extent and affects the occurrence of SAP.

Studies have shown a good association between several radiomics features and clinical stroke outcomes, such as prognosis and recurrence [18]. Currently, the radiomics features has been certified to improve the prediction ability of prognosis prediction. Tang et al. [48] found an association between specific morphology radiomics features and stroke recurrence in patients with symptomatic intracranial atherosclerotic stenosis. With the addition of radiomics features, the AUC of the prediction model was increased by 11.7% and 17% in the training and validation sets, respectively. Zhou et al. [49] demonstrated that the radiomics features performed well in predicting AIS outcomes. With the addition of radiomics features, the AUC of the prediction model was increased by 10.1% and 10.6% in the training and validation sets, respectively. However, relatively few studies have used radiomics features to predict the risk of complications following AIS. Immunological changes are associated with an increased tendency to respiratory infections [13]. And neuroanatomical correlates are associated with immunological changes after stroke and increased risk of infection, so it is easy to develop SAP [16]. An activation of the sympathetic nervous system is the main immunosuppressive mechanism leading to a high incidence of infections after stroke [50]. Studies have revealed that significant correlations with texture features and neural density in the side of the hippocampus contralateral to the ischemic area. These preliminary results suggest that texture features

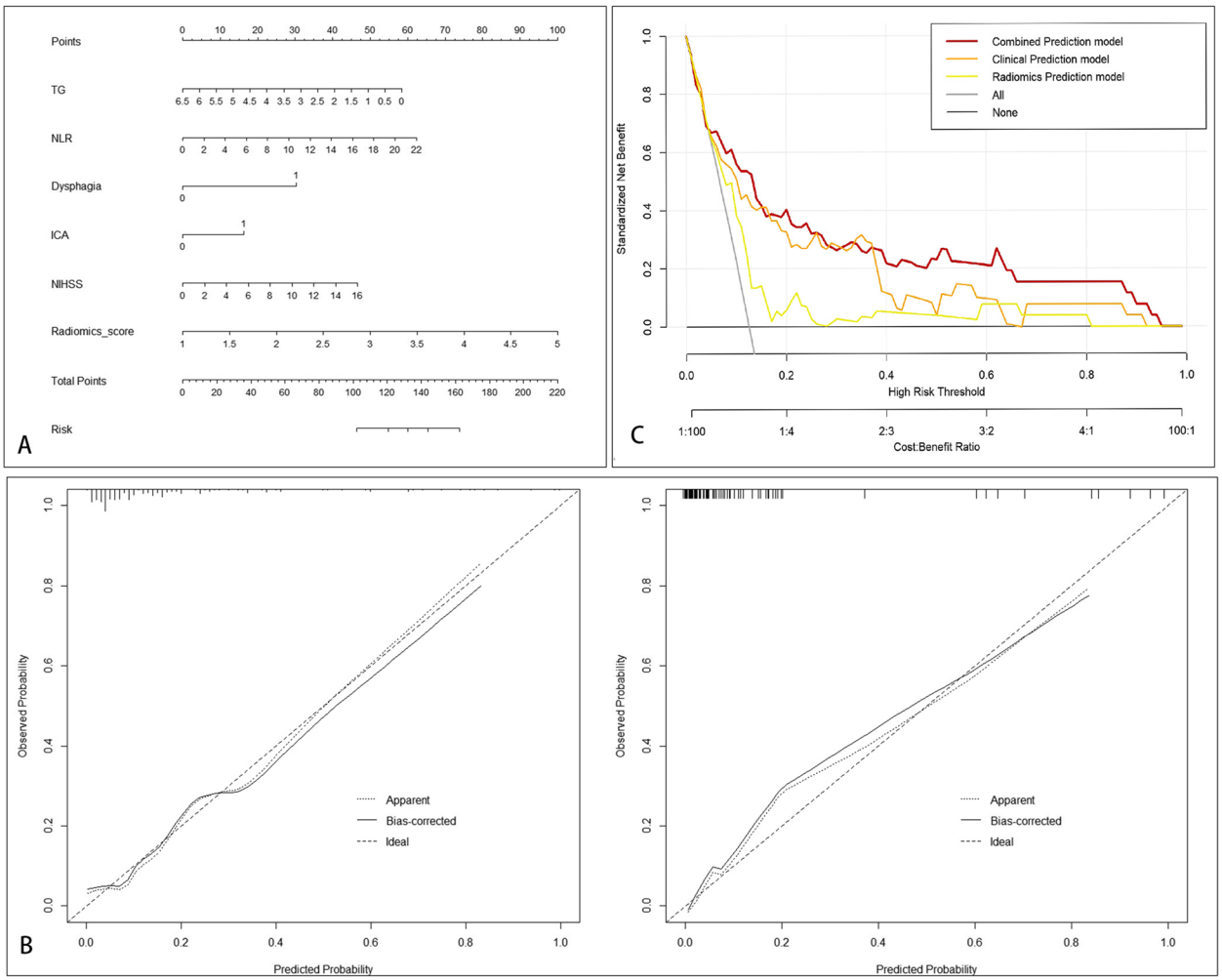

Fig. 9 Nomogram of the combined prediction SAP model. **A** The nomogram. **B** The calibration curves for the training and validation nomograms. **C** The decision curve for the nomogram

Table 5 Subgroup analysis of AUCs using the Delong test

Subgroups divided by	AUC	*P* (versus overall set)
Age		
Age > = 60	0.857	0.694
Age < 60	0.822	0.927
Sex		
Male	0.820	0.914
Female	0.842	0.928
BMI		
BMI > = 24	0.811	0.878
BMI < 24	0.837	0.942
Stroke severity on admission		
Normal or nearly normal (NIHSS score 0–1)	0.853	0.804
Mild stroke (NIHSS score 2–4)	0.857	0.460
Moderate stroke (NIHSS score 4–15)	0.775	0.581

can reflect microscopic changes that occur post-stroke, even in an area spared by ischemia [29]. Therefore, we believe that the extracted radiomics features, belonging to the texture features, can reflect the microscopic changes that occur after a stroke and provide a good representation of neural alterations caused by low immunity. It may potentially be used to predict the risk of developing infections after AIS. In this study, we used the PyRadiomics software version 3.0.1 to extract radiomics features from the manually segmented brain lesions [18]. A total of 1041 radiomics features were obtained, of which 10 were identified as highly predictive of SAP. The majority of these features belonged to the wavelet feature cluster. The wavelet feature cluster measures asymmetry around the mean, which represents the tissue damage caused by the infarct. A study reported that this type of features might be associated with complications due to other pathological changes [49]. Among these features,

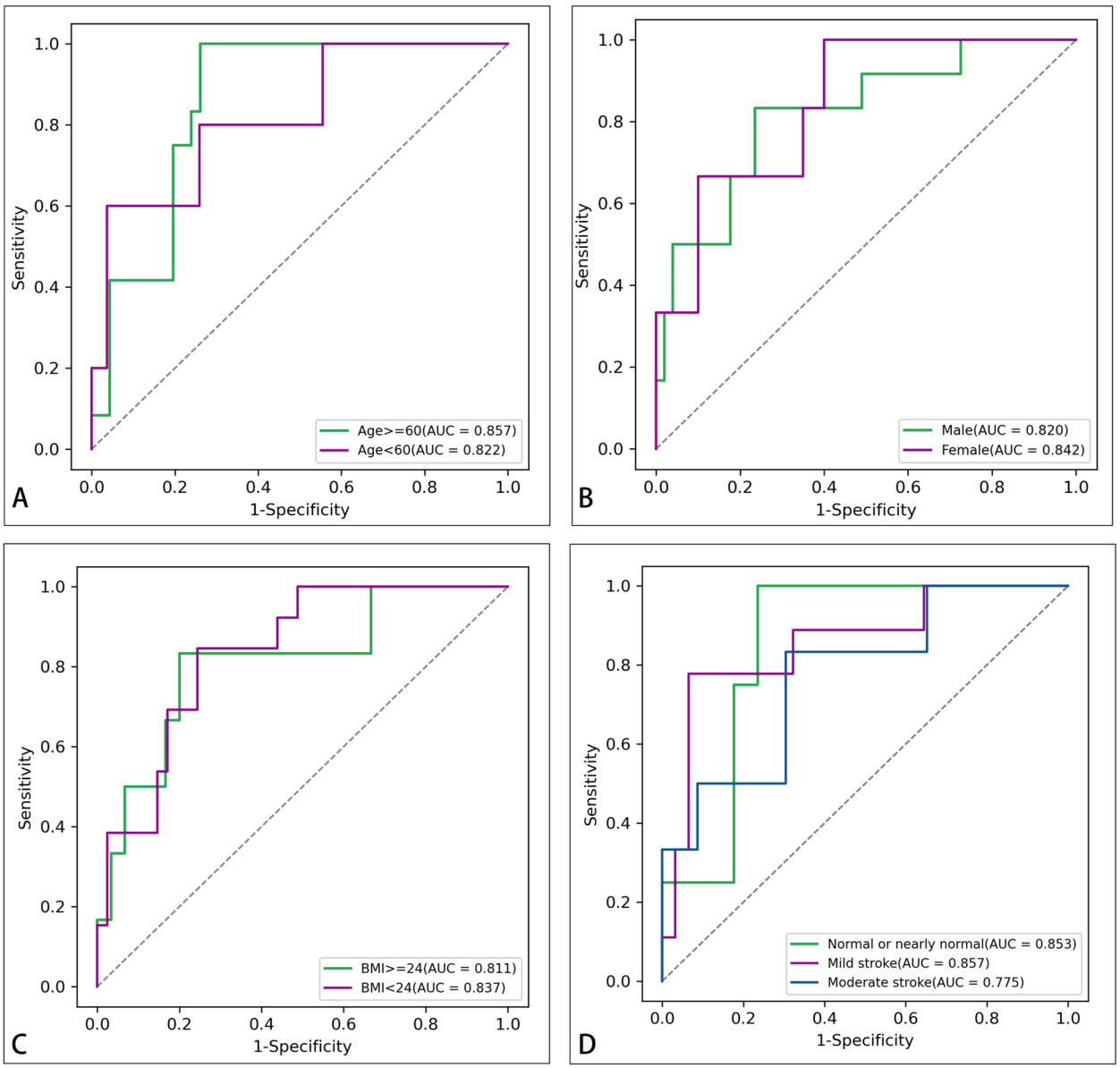

Fig. 10 Subgroup analysis of the combined model. After dividing by the age (**A**), sex (**B**), BMI (**C**), and stroke severity on admission (**D**)

LowGrayLevelZoneEmphasis is a feature used to describe the distribution of gray levels in an image, and in MRI images of stroke patients, lesion site usually shows different gray levels, which reflects the difference in density between the lesion site and the surrounding normal site. Higher LowGrayLevelZoneEmphasis values indicate that areas of lower gray levels are more prominent around the lesion site, which may suggest pathological changes in the contours or margins of the infarcts, reflecting heterogeneity of the lesion site, which may be associated with SAP. Cluster Prominence represents the cluster significance and is a measure of GLCM skewness and asymmetry, which was associated with stroke prognosis in previous studies [51], may be related to the occurrence of pneumonia. However, more research is required to understand the molecular mechanisms involved behind the development of this feature.

Consistent with previous studies, NLR, dysphagia, and NIHSS score were identified as independent predictors of SAP [1, 42, 52–54]. In addition, the stenosis location (ICA) and low TG were also identified as independent risk factors for predicting SAP. Chlamydia pneumoniae infection can also promote the development of atherosclerosis [55], Cao J et al. found that

84.0% of Chinese patients with carotid atherosclerotic plaques tested positive for chlamydia pneumonia-specific antigens [56]. As atherosclerotic plaques grow larger, leading to the narrowing of the arteries [57], the body's immunity system is weakened, leading to an increased risk of infections [16]. A previous study reported that when compared to MCA, the ICA causes larger infarcts, thus increasing the risk of SAP [58]. Our study found that patients with ICA stenosis were more likely to develop SAP, and this relationship persisted after adjustment for confounding factors. Patients with ICA stenosis had larger infarct volumes, and larger infarct volumes can affect multiple brain functions and impair immunity, ultimately leading to functional impairment and increased susceptibility to infections [16]. TGs are a potential source of arachidonic acids. The lipases and cyclooxygenase found in the lipid droplets of macrophages can catalyze the esterification of arachidonic acid to gradually transform it into eicosanoids compounds [59, 60]. These compounds are important lipid mediators of inflammation, and have an important role in balancing the extent of the inflammatory response [61]. Some studies have shown that when the concentration of TG is high, the TG-rich lipoprotein can combine with lipopolysaccharide to exert immune regulation on cells crucial for hosting the immune defense [62], thus reducing the risk of SAP. The same association was not reported in other studies [63, 64]. Therefore, further research is recommended to confirm the specific relationship between TG and SAP.

Our study has some limitations that have to be acknowledged. Since this study was based on data extracted retrospectively, the model's prediction accuracy needs to be validated prospectively. The use of single-agency data may lead to issues of geographic specificity and representativeness of the sample, a limitation that may restrict our generalizations about different groups. Therefore, in future studies, we will actively explore the possibility of external validation to enhance the reliability and generalizability of the study. In addition, the effect of treatment during hospitalization was not taken into account in this model. Finally, the combined model had a high NPV and a low PPV, possibly due to the low incidence of SAP in our cohort (SAP: 39/298, 13.1%).

Conclusion

The addition of the radiomics features to the clinical model improved the prediction of SAP in AIS patients, which verified its feasibility. The proposed nomogram could identify patients at risk of developing SAP and thus provide timely interventions.

Acknowledgements
Thanks to all the members participated in this study.

Authors' contributions
HL and JL wrote the manuscript. YC, BW, JL, MH, YW, WJ, PY, RC, XW, JK, HX and JT critically revised the study. YY supervised the manuscript. All authors contributed to the article and approved the submitted version.

Funding
This study was supported by the National Natural Science Foundation of China (No. 81960609), Jiangxi Provincial Key R&D Plan(20223BBH80013), the Second Affiliated Hospital of Nanchang University Funding Program (No. 2021efyB03), the National Key R&D Program of China (No. 2020YFC2002901, No. 2018YFC1312902), and the Applied Research Cultivation Program of Jiangxi Province (No. 20212BAG70029).

Availability of data and materials
The data that support the findings of this study are available on request from the corresponding author. The data are not publicly available due to privacy or ethical restrictions.

Declarations

Ethics approval and consent to participate
The study was approved by the Medical Ethics Committee of the Second Affiliated Hospital of Nanchang University: (2018) Medical Research Review No.04. and written informed consent was obtained from all patients participating in this study. All methods were carried out in accordance with relevant guidelines and regulation.

Consent for publication
Not applicable.

Competing interests
The authors declare no competing interests.

Author details
[1]Department of Medical Big Data Research Centre, The Second Affiliated Hospital of Nanchang University, 1MinDe Road, Nanchang 330006, P.R. China. [2]School of Public Health, Jiangxi Provincial Key Laboratory of Preventive Medicine, Nanchang University, Nanchang, China. [3]Department of Neurology, The Second Affiliated Hospital of Nanchang University, 1MinDe Road, Nanchang 330006, P.R. China.

Received: 17 September 2023 Accepted: 8 January 2024
Published online: 25 January 2024

References

1. Finlayson O, Kapral M, Hall R, Asllani E, Selchen D, Saposnik G, et al. Risk factors, inpatient care, and outcomes of pneumonia after ischemic stroke. Neurology. 2011;77(14):1338–45.
2. Koennecke HC, Belz W, Berfelde D, Endres M, Fitzek S, Hamilton F, et al. Factors influencing in-hospital mortality and morbidity in patients treated on a stroke unit. Neurology. 2011;77(10):965–72.
3. Katzan IL, Cebul RD, Husak SH, Dawson NV, Baker DWK, et al. The effect of pneumonia on mortality among patients hospitalized for acute stroke. Neurology. 2003;60(4):620–5.
4. Collaborators GBDLRoS, Feigin VL, Nguyen G, Cercy K, Johnson CO, Alam T, et al. Global, Regional, and Country-Specific Lifetime Risks of Stroke, 1990 and 2016. N Engl J Med. 2018;379(25):2429–37.
5. Vermeij FH, Scholte op Reimer WJ, de Man P, van Oostenbrugge RJ, Franke CL, de Jong G, et al. Stroke-associated infection is an independent risk factor for poor outcome after acute ischemic stroke: data from the Netherlands Stroke Survey. Cerebrovasc Dis. 2009;27(5):465–71.
6. Forti P, Maioli F, Procaccianti G, Nativio V, Lega MV, Coveri M, et al. Independent predictors of ischemic stroke in the elderly: prospective data from a stroke unit. Neurology. 2013;80(1):29–38.

7. Hoffmann S, Malzahn U, Harms H, Koennecke HC, Berger K, Kalic M, et al. Development of a clinical score (A2DS2) to predict pneumonia in acute ischemic stroke. Stroke. 2012;43(10):2617–23.
8. Smith CJ, Bray BD, Hoffman A, Meisel A, Heuschmann PU, Wolfe CD, et al. Can a novel clinical risk score improve pneumonia prediction in acute stroke care? A UK multicenter cohort study. J Am Heart Assoc. 2015;4(1):e001307.
9. Zhang R, Ji R, Pan Y, Jiang Y, Liu G, Wang Y, et al. External Validation of the Prestroke Independence, Sex, Age, National Institutes of Health Stroke Scale Score for Predicting Pneumonia After Stroke Using Data From the China National Stroke Registry. J Stroke Cerebrovasc Dis. 2017;26(5):938–43.
10. Ni J, Shou W, Wu X, Sun J. Prediction of stroke-associated pneumonia by the A2DS2, AIS-APS, and ISAN scores: a systematic review and meta-analysis. Expert Rev Respir Med. 2021;15(11):1461–72.
11. Vert C, Parra-Farinas C, Rovira A. MR imaging in hyperacute ischemic stroke. Eur J Radiol. 2017;96:125–32.
12. Powers WJ, Rabinstein AA, Ackerson T, Adeoye OM, Bambakidis NC, Becker K, et al. Guidelines for the Early Management of Patients With Acute Ischemic Stroke: 2019 Update to the 2018 Guidelines for the Early Management of Acute Ischemic Stroke: A Guideline for Healthcare Professionals From the American Heart Association/American Stroke Association. Stroke. 2019;50(12):e344–418.
13. Iadecola C, Anrather J. The immunology of stroke: from mechanisms to translation. Nat Med. 2011;17(7):796–808.
14. Hug A, Dalpke A, Wieczorek N, Giese T, Lorenz A, Auffarth G, et al. Infarct volume is a major determiner of post-stroke immune cell function and susceptibility to infection. Stroke. 2009;40(10):3226–32.
15. Urra X, Chamorro A. Stroke-induced immunodepression is a marker of severe brain damage. Stroke. 2010;41(2):e110 (author reply e1).
16. Urra X, Laredo C, Zhao Y, Amaro S, Rudilosso S, Renu A, et al. Neuroanatomical correlates of stroke-associated infection and stroke-induced immunodepression. Brain Behav Immun. 2017;60:142–50.
17. Yu Y, Xia T, Tan Z, Xia H, He S, Sun H, et al. A^2DS^2 Score Combined With Clinical and Neuroimaging Factors Better Predicts Stroke-Associated Pneumonia in Hyperacute Cerebral Infarction. Front Neurol. 2022;13:800614.
18. Chen Q, Xia T, Zhang M, Xia N, Liu J, Yang Y. Radiomics in Stroke Neuroimaging: Techniques, Applications, and Challenges. Aging Dis. 2021;12(1):143–54.
19. Dong D, Fang MJ, Tang L, Shan XH, Gao JB, Giganti F, et al. Deep learning radiomic nomogram can predict the number of lymph node metastasis in locally advanced gastric cancer: an international multicenter study. Ann Oncol. 2020;31(7):912–20.
20. Dong D, Tang L, Li ZY, Fang MJ, Gao JB, Shan XH, et al. Development and validation of an individualized nomogram to identify occult peritoneal metastasis in patients with advanced gastric cancer. Ann Oncol. 2019;30(3):431–8.
21. Meng L, Dong D, Chen X, Fang M, Wang R, Li J, et al. 2D and 3D CT Radiomic Features Performance Comparison in Characterization of Gastric Cancer: A Multi-Center Study. IEEE J Biomed Health Inform. 2021;25(3):755–63.
22. Zhang L, Dong D, Zhang W, Hao X, Fang M, Wang S, et al. A deep learning risk prediction model for overall survival in patients with gastric cancer: A multicenter study. Radiother Oncol. 2020;150:73–80.
23. Peter R, Korfiatis P, Blezek D, Oscar Beitia A, Stepan-Buksakowska I, Horinek D, et al. A quantitative symmetry-based analysis of hyperacute ischemic stroke lesions in noncontrast computed tomography. Med Phys. 2017;44(1):192–9.
24. Sikio M, Kolhi P, Ryymin P, Eskola HJ, Dastidar P. MRI Texture Analysis and Diffusion Tensor Imaging in Chronic Right Hemisphere Ischemic Stroke. J Neuroimaging. 2015;25(4):614–9.
25. Xie H, Ma S, Wang X, Zhang X. Noncontrast computer tomography-based radiomics model for predicting intracerebral hemorrhage expansion: preliminary findings and comparison with conventional radiological model. Eur Radiol. 2020;30(1):87–98.
26. Kanazawa T, Takahashi S, Minami Y, Jinzaki M, Toda M, Yoshida K. Early prediction of clinical outcomes in patients with aneurysmal subarachnoid hemorrhage using computed tomography texture analysis. J Clin Neurosci. 2020;71:144–9.
27. Su JH, Meng LW, Dong D, Zhuo WY, Wang JM, Liu LB, et al. Noninvasive model for predicting future ischemic strokes in patients with silent lacunar infarction using radiomics. BMC Med Imaging. 2020;20(1):77.
28. Tang TY, Jiao Y, Cui Y, Zhao DL, Zhang Y, Wang Z, et al. Penumbra-based radiomics signature as prognostic biomarkers for thrombolysis of acute ischemic stroke patients: a multicenter cohort study. J Neurol. 2020;267(5):1454–63.
29. Betrouni N, Yasmina M, Bombois S, Petrault M, Dondaine T, Lachaud C, et al. Texture Features of Magnetic Resonance Images: an Early Marker of Post-stroke Cognitive Impairment. Transl Stroke Res. 2020;11(4):643–52.
30. Mendelson SJ, Prabhakaran S. Diagnosis and Management of Transient Ischemic Attack and Acute Ischemic Stroke: A Review. JAMA. 2021;325(11):1088–98.
31. Stroke--1989. Recommendations on stroke prevention, diagnosis, and therapy. Report of the WHO Task Force on Stroke and other Cerebrovascular Disorders. Stroke. 1989;20(10):1407–31.
32. Smith CJ, Kishore AK, Vail A, Chamorro A, Garau J, Hopkins SJ, et al. Diagnosis of Stroke-Associated Pneumonia: Recommendations From the Pneumonia in Stroke Consensus Group. Stroke. 2015;46(8):2335–40.
33. Saver JL, Chaisinanunkul N, Campbell BCV, Grotta JC, Hill MD, Khatri P, et al. Standardized Nomenclature for Modified Rankin Scale Global Disability Outcomes: Consensus Recommendations From Stroke Therapy Academic Industry Roundtable XI. Stroke. 2021;52(9):3054–62.
34. Regenhardt RW, Young MJ, Etherton MR, Das AS, Stapleton CJ, Patel AB, et al. Toward a more inclusive paradigm: thrombectomy for stroke patients with pre-existing disabilities. J Neurointerv Surg. 2021;13(10):865–8.
35. Koo TK, Li MY. A Guideline of Selecting and Reporting Intraclass Correlation Coefficients for Reliability Research. J Chiropr Med. 2016;15(2):155–63.
36. Zwanenburg A, Vallieres M, Abdalah MA, Aerts H, Andrearczyk V, Apte A, et al. The Image Biomarker Standardization Initiative: Standardized Quantitative Radiomics for High-Throughput Image-based Phenotyping. Radiology. 2020;295(2):328–38.
37. Jiang M, Li C, Tang S, Lv W, Yi A, Wang B, et al. Nomogram Based on Shear-Wave Elastography Radiomics Can Improve Preoperative Cervical Lymph Node Staging for Papillary Thyroid Carcinoma. Thyroid. 2020;30(6):885–97.
38. Tibshirani R. Regression shrinkage and selection via the lasso: a retrospective. Journal of the Royal Statistical Society: Series B (Statistical Methodology). 2011;73(3):273–82.
39. Kramer AA, Zimmerman JE. Assessing the calibration of mortality benchmarks in critical care: The Hosmer-Lemeshow test revisited. Crit Care Med. 2007;35(9):2052–6.
40. Fitzgerald M, Saville BR, Lewis RJ. Decision curve analysis. JAMA. 2015;313(4):409–10.
41. Teh WH, Smith CJ, Barlas RS, Wood AD, Bettencourt-Silva JH, Clark AB, et al. Impact of stroke-associated pneumonia on mortality, length of hospitalization, and functional outcome. Acta Neurol Scand. 2018;138(4):293–300.
42. Walter U, Knoblich R, Steinhagen V, Donat M, Benecke R, Kloth A. Predictors of pneumonia in acute stroke patients admitted to a neurological intensive care unit. J Neurol. 2007;254(10):1323–9.
43. Zhao D, Zhu J, Cai Q, Zeng F, Fu X, Hu K. The value of diffusion weighted imaging-alberta stroke program early CT score in predicting stroke-associated pneumonia in patients with acute cerebral infarction: a retrospective study. PeerJ. 2022;10:e12789.
44. Li X, Wu M, Sun C, Zhao Z, Wang F, Zheng X, et al. Using machine learning to predict stroke-associated pneumonia in Chinese acute ischaemic stroke patients. Eur J Neurol. 2020;27(8):1656–63.
45. Reid AT, van Norden AG, de Laat KF, van Oudheusden LJ, Zwiers MP, Evans AC, et al. Patterns of cortical degeneration in an elderly cohort with cerebral small vessel disease. Hum Brain Mapp. 2010;31(12):1983–92.
46. Okada R, Okada T, Okada A, Muramoto H, Katsuno M, Sobue G, et al. Severe brain atrophy in the elderly as a risk factor for lower respiratory tract infection. Clin Interv Aging. 2012;7:481–7.
47. Kwah LK, Diong J. National Institutes of Health Stroke Scale (NIHSS). J Physiother. 2014;60(1):61.
48. Tang M, Gao J, Ma N, Yan X, Zhang X, Hu J, et al. Radiomics Nomogram for Predicting Stroke Recurrence in Symptomatic Intracranial Atherosclerotic Stenosis. Front Neurosci. 2022;16:851353.

49. Zhou Y, Wu D, Yan S, Xie Y, Zhang S, Lv W, et al. Feasibility of a Clinical-Radiomics Model to Predict the Outcomes of Acute Ischemic Stroke. Korean J Radiol. 2022;23(8):811–20.
50. Prass K, Meisel C, Hoflich C, Braun J, Halle E, Wolf T, et al. Stroke-induced immunodeficiency promotes spontaneous bacterial infections and is mediated by sympathetic activation reversal by poststroke T helper cell type 1-like immunostimulation. J Exp Med. 2003;198(5):725–36.
51. Wang H, Sun Y, Ge Y, Wu PY, Lin J, Zhao J, et al. A Clinical-Radiomics Nomogram for Functional Outcome Predictions in Ischemic Stroke. Neurol Ther. 2021;10(2):819–32.
52. Nam KW, Kim TJ, Lee JS, Kwon HM, Lee YS, Ko SB, et al. High Neutrophil-to-Lymphocyte Ratio Predicts Stroke-Associated Pneumonia. Stroke. 2018;49(8):1886–92.
53. Bray BD, Smith CJ, Cloud GC, Enderby P, James M, Paley L, et al. The association between delays in screening for and assessing dysphagia after acute stroke, and the risk of stroke-associated pneumonia. J Neurol Neurosurg Psychiatry. 2017;88(1):25–30.
54. Eltringham SA, Kilner K, Gee M, Sage K, Bray BD, Smith CJ, et al. Factors Associated with Risk of Stroke-Associated Pneumonia in Patients with Dysphagia: A Systematic Review. Dysphagia. 2019;35(5):735–44.
55. Evani SJ, Dallo SF, Ramasubramanian AK. Biophysical and Biochemical Outcomes of Chlamydia pneumoniae Infection Promotes Pro-atherogenic Matrix Microenvironment. Front Microbiol. 2016;7:1287.
56. Cao J, Mao Y, Dong B, Guan W, Shi J, Wang S. Detection of specific Chlamydia pneumoniae and cytomegalovirus antigens in human carotid atherosclerotic plaque in a Chinese population. Oncotarget. 2017;8(33):55435–42.
57. Chistiakov DA, Melnichenko AA, Myasoedova VA, Grechko AV, Orekhov AN. Mechanisms of foam cell formation in atherosclerosis. J Mol Med (Berl). 2017;95(11):1153–65.
58. Zhang C, Wang Y, Zhao X, Liu L, Wang C, Li Z, et al. Clinical, imaging features and outcome in internal carotid artery versus middle cerebral artery disease. PLoS ONE. 2019;14(12):e0225906.
59. Menon D, Singh K, Pinto SM, Nandy A, Jaisinghani N, Kutum R, et al. Quantitative Lipid Droplet Proteomics Reveals Mycobacterium tuberculosis Induced Alterations in Macrophage Response to Infection. ACS Infect Dis. 2019;5(4):559–69.
60. Dvorak AM, Morgan E, Schleimer RP, Ryeom SW, Lichtenstein LM, Weller PF. Ultrastructural immunogold localization of prostaglandin endoperoxide synthase (cyclooxygenase) to non-membrane-bound cytoplasmic lipid bodies in human lung mast cells, alveolar macrophages, type II pneumocytes, and neutrophils. J Histochem Cytochem. 1992;40(6):759–69.
61. Tobin DM, Roca FJ, Oh SF, McFarland R, Vickery TW, Ray JP, et al. Host genotype-specific therapies can optimize the inflammatory response to mycobacterial infections. Cell. 2012;148(3):434–46.
62. Barcia AM, Harris HW. Triglyceride-rich lipoproteins as agents of innate immunity. Clin Infect Dis. 2005;41(Suppl 7):S498-503.
63. Masana L, Correig E, Ibarretxe D, Anoro E, Arroyo JA, Jerico C, et al. Low HDL and high triglycerides predict COVID-19 severity. Sci Rep. 2021;11(1):7217.
64. Fang J, Wang F, Song H, Wang Z, Zuo Z, Cui H, et al. AMPKalpha pathway involved in hepatic triglyceride metabolism disorder in diet-induced obesity mice following Escherichia coli Infection. Aging (Albany NY). 2018;10(11):3161–72.

Publisher's Note